Title

Trap Passivation in Indium-Based Quantum Dots through Surface Fluorination: Mechanism and Applications.

Journal

ACS nano, 12(11)

ISSN

1936-0851

Authors

Kim, Tae-Gon
Zherebetskyy, Danylo
Bekenstein, Yehonadav
et al.

Publication Date

2018-11-01

DOI

10.1021/acsnano.8b06692

Peer reviewed

ACS NANO
Cite This: ACS Nano XXXX, XXX, XXX–XXX
www.acsnano.org

ARTICLE

Trap Passivation in Indium-Based Quantum Dots through Surface Fluorination: Mechanism and Applications

Tae-Gon Kim,[†,‡] Danylo Zherebetskyy,[§] Yehonadav Bekenstein,[‡,§,⊥] Myoung Hwan Oh,[‡,§] Lin-Wang Wang,[§] Eunjoo Jang,[*,†] and A. Paul Alivisatos[*,‡,§,∥]

[†]Inorganic Materials Lab., Samsung Advanced Institute of Technology, Suwon 443-803, Korea
[‡]Department of Chemistry, University of California, Berkeley, Berkeley, California 94720, United States
[§]Materials Sciences Division, Lawrence Berkeley National Laboratory, Berkeley, California 94720, United States
[∥]Kavli Energy NanoScience Institute, Berkeley, California 94720, United States

Supporting Information

ABSTRACT: **Treatment of InP colloidal quantum dots (QDs) with hydrofluoric acid (HF) has been an effective method to improve their photoluminescence quantum yield (PLQY) without growing a shell. Previous work has shown that this can occur through the dissolution of the fluorinated phosphorus and subsequent passivation of indium on the reconstructed surface by excess ligands. In this article, we demonstrate that very significant luminescence enhancements occur at lower HF exposure though a different mechanism. At lower exposure to HF, the main role of the fluoride ions is to directly passivate the surface indium dangling bonds in the form of atomic ligands. The PLQY enhancement in this case is accompanied by red shifts of the emission and absorption peaks rather than blue shifts caused by etching as seen at higher exposures. Density functional theory shows that the surface fluorination is thermodynamically preferred and that the observed spectral characteristics might be due to greater exciton delocalization over the outermost surface layer of the InP QDs as well as alteration of the optical oscillator strength by the highly electronegative fluoride layer. Passivation of surface indium with fluorides can be applied to other indium-based QDs. PLQY of InAs QDs could also be increased by an order of magnitude *via* fluorination. We fabricated fluorinated InAs QD-based electrical devices exhibiting improved switching and higher mobility than those of 1,2-ethanedithiol cross-linked QD devices. The effective surface passivation eliminates persistent photoconductivity usually found in InAs QD-based solid films.**

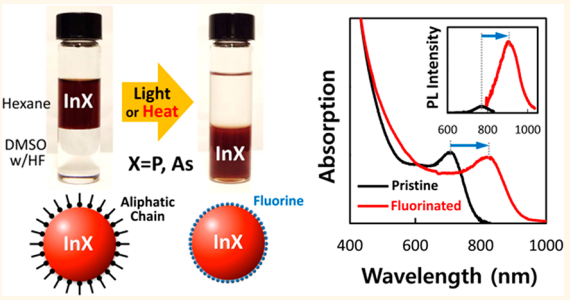

KEYWORDS: *indium phosphide, quantum dots, fluorine, etching, atomic ligand, indium arsenide*

In semiconductor colloidal quantum dots (QDs) with a large surface to volume ratio, passivation of surface defects is key to obtain high-quality materials for optoelectronic devices.[1−8] The most common effective method for surface passivation is the growth of a wide-band gap shell coating.[9−14] However, this approach diminishes carrier mobility, since the shell hampers charge transport between QDs, which is required for applications in solar cells, photodetectors, and field-effect transistors (FETs).[3−5,8,15−21] Alternatively, atomic or short-chain molecular ligands can passivate the surface defects and promote spatial proximity and electronic coupling between QDs. Various types of chemical units such as bifunctional organic molecules, inorganic molecules, single ions, and metal chalcogenide complexes have been used as ligands for QD thin films.[3−5,8,15−21] Cd- and Pb-based QDs have been extensively studied, and their passivation methods are well-developed to minimize surface imperfections.[2−8] In fact, Cd- and Pb-chalcogenide QD solid films have shown excellent electronic qualities that are suitable for existing conventional devices.[4,5,16−21] These are attributed to their ionic bonding characters that are highly tolerant to the in-gap states (IGS) when the global charge neutrality or chemical stoichiometry is satisfied.[2,22,23] Unfortunately, Cd- and Pb-based QD devices are frequently prohibited for some commercial uses by restriction of hazardous substances directives, owing to their potential harmful effects on health and the environment.[24,25] Accordingly, there is a high demand

Received: September 1, 2018
Accepted: October 16, 2018
Published: October 16, 2018

DOI: 10.1021/acsnano.8b06692
ACS Nano XXXX, XXX, XXX–XXX

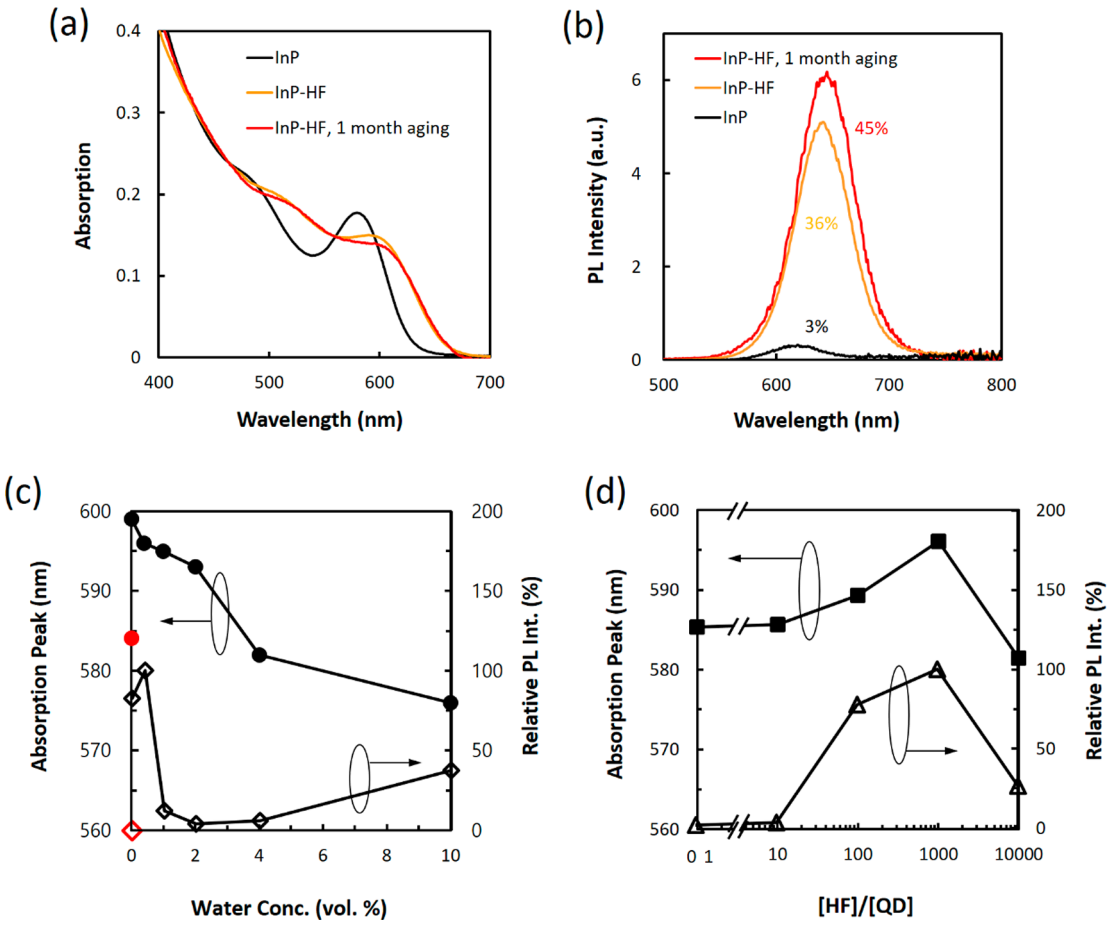

Figure 1. (a) Optical absorption and (b) photoluminescence (PL) spectra of pristine InP QDs (black), HF-treated InP QDs (orange), and HF-treated InP QDs after 1-month aging at room temperature (red) normalized by the optical density at 450 nm as an excitation wavelength. Absorption peak positions and relative PL intensities of HF-treated InP QDs as functions of (c) distilled water concentrations (0, 0.4, 1, 2, 4, and 10 vol %) at [HF]/[QD] = 1000 and (d) [HF]/[QD] = 0, 10, 100, 1000, and 10000 without adding water. Red solid circle and vacant diamond in (c) indicate the absorption peak position and the relative PL intensity before the HF treatment, respectively.

for alternative materials that do not involve heavy metal ions for practical applications. On one hand, among various candidates, III−V QDs such as InP or InAs have been mostly considered owing to their relatively low toxicity as well as their optical characteristics being comparable to Cd- or Pb-based QDs.[26−30] On the other hand, III−V QDs are easily oxidized and present weak electronic tolerance to surface defects due to their high covalent character.[26,31−33] In brief, it is intrinsically more challenging to handle III−V QDs and to improve their quality to acceptable levels.

InP is the III−V material with the highest level of colloidal synthesis development, owing in part to its ability to shift across the visible spectrum with quantum confinement. One of the most effective ways to improve the photoluminescence (PL) of InP QDs is HF etching primarily introduced by Mićić *et al.* in 1996.[34] A photoluminescence quantum yield (PLQY) of InP QD higher than 40% can be achieved by a room-temperature HF reaction. Talapin *et al.* showed that HF etching of InP QDs is a photochemical reaction.[35] Adams *et al.*[36,37] suggested a more detailed mechanism involving the photochemical removal of P dangling bonds and the subsequent passivation of the reconstructed In dangling bonds by residual ligands such as trioctylphosphine oxide, based on synchrotron X-ray photoelectron spectroscopy (XPS) analyses. Here we present evidence that PLQY enhancement by HF treatment can arise at low concentration through passivation of indium dangling bonds by fluoride ions acting as atomic ligands before HF exposure produces the photochemical etching as observed previously. Owing to the strong electron-withdrawing property of fluoride on the surface, the subsequent optical property becomes distinct in comparison to those of as-synthesized InP and ZnS-shell-passivated InP QDs. Following these ideas, we also observed that the PLQY of InAs QDs can also be improved by HF treatment again because the fluoride ions effectively passivate surface indium sites.

RESULTS AND DISCUSSION

Photophysical Properties of HF-Treated InP QDs. Figure 1(a,b) show the absorption and PL spectra of InP QDs before and after HF treatment. The PLQY of InP QDs is enhanced from 3% to 36% under AM1.5 white light irradiation for 30 min after the addition of a dilute HF to InP QD solution ([HF]/[QD] = 5000:1). It is generally accepted that HF induces the QD etching, causing blue shifts of the optical absorption and PL peaks.[34−41] However, we observed significant red shifts of absorption and PL peaks at some HF exposure. The second derivatives of the absorption spectra in Figure S1 show more clearly the red shifts of both the first (Δ = 0.08 eV) and the second (Δ = 0.16 eV) peaks. Change of the feature around the absorption edge results from the larger red

DOI: 10.1021/acsnano.8b06692
ACS Nano XXXX, XXX, XXX−XXX

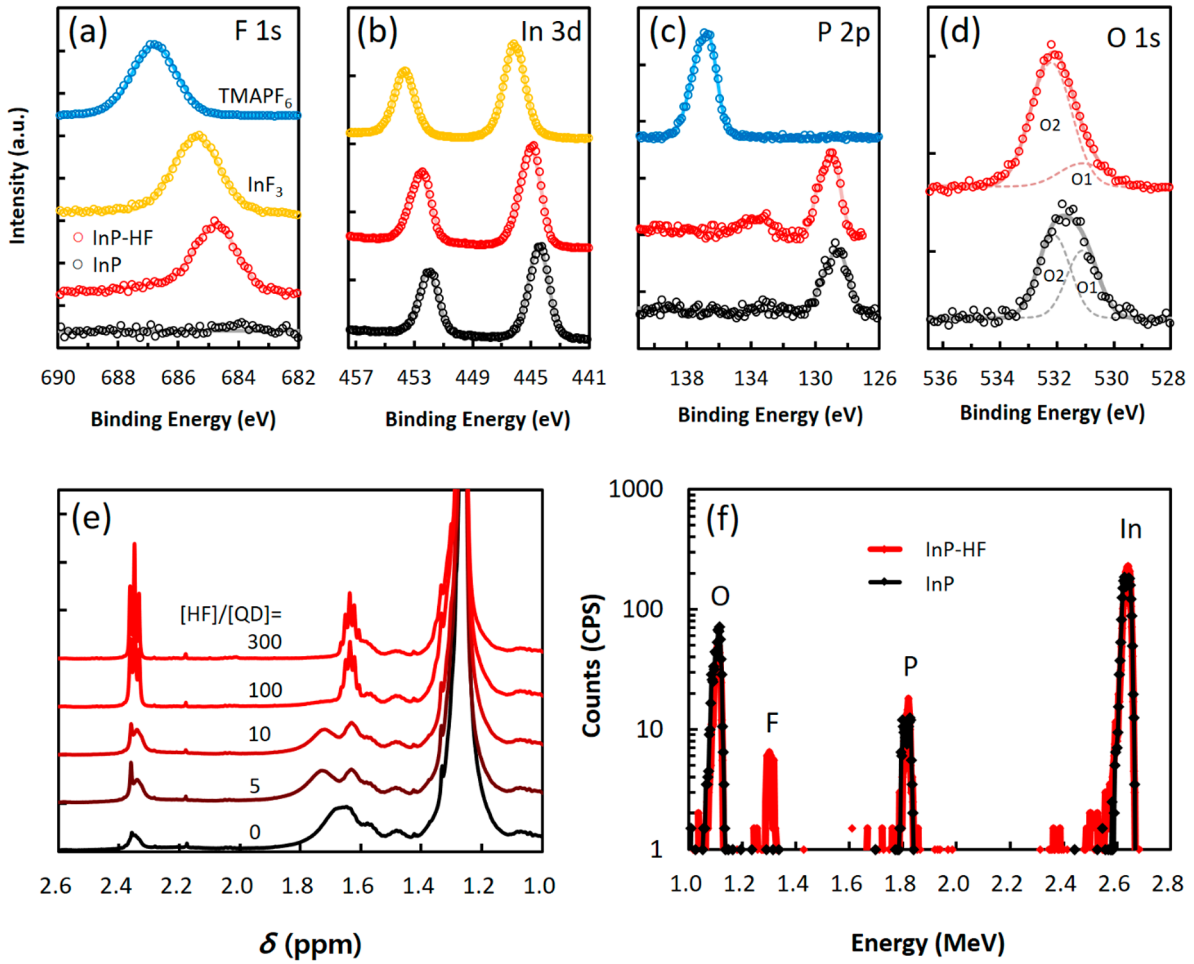

Figure 2. (a) F 1s, (b) In 3d, (c) P 2p, and (d) O 1s XPS spectra of pristine InP (black), HF-treated InP (red), InF_3 (orange), and trimethylammonium hexafluorophosphate ($TMAPF_6$, blue). Measured and fitted data are expressed as vacant circles and solid lines, respectively. (e) ^{1}H NMR spectra of InP QDs treated with various HF concentrations as [HF]/[QD] = 0, 5, 10, 100, and 300 and (f) RBS curves of pristine (black) and HF-treated InP (red) QDs.

shift of the second peak than the first and their broadening as well. Additional red shifts and PLQY improvement to 45% in samples stored for 1 month under ambient conditions corroborate that there was negligible etching despite the significant PLQY enhancement. If the red shift of 0.08 eV originates from the increase of QD sizes, the size change should be about 0.3−0.4 nm.[42] However, almost constant QD sizes before and after the HF treatment obtained from scanning transmission electron microscope images suggest that the change of the absorption edge might not result from the simple morphological change (Figure S2 in the SI). To understand this new HF treatment regime, we varied the experimental conditions for the HF treatment and found two parameters that control the peak shifts. First, concentrations of distilled water in the solvent can affect the degree of etching. Distilled water has been intentionally added as a cosolvent for the HF reaction in previous studies.[34−41] As shown in Figures 1(c) and S3 in the SI, the HF treatment induces red shifts of the absorption peak from 584 nm to 599 nm without additional water. The effect of water from the 48 wt % HF aqueous solution is negligible, since it is just 0.005 vol % of the total QD solution at the tested HF concentration as [HF]/[QD] = 1000. The red shift gradually decreases along with increasing water concentrations, and finally it shows a blue shift from the initial 584 nm to 576 nm at 10 vol % water. Another condition for the etching is a high concentration of HF. The blue shift of the absorption peak from 585 nm to 581 nm could be found also at [HF]/[QD] = 10 000 even without additional water, although the red shifts consistently increase to some extent ([HF]/[QD] ≤ 1000) (Figures 1(d) and S4 in the SI). These results suggest that the etching of InP QDs could occur in some chemically reactive environments and not be the inevitable consequence of the HF treatment. Instead, we observe the regime of relatively low HF and water concentrations where the HF treatment induces the red shifts of the absorption and PL peaks coupled with a very significant PL quantum yield enhancement.

Surface Chemistry of HF-Treated InP QDs. We investigated the chemical change caused by the HF treatment ([HF]/[QD] = 5000) to understand the structural origin of the photophysical change discussed above. In the XPS spectra shown in Figure 2(a), the F 1s peak is detected only in the HF-treated QDs even after washing twice with acetonitrile, indicating that fluoride is chemically bound to InP QDs. The peak position at 684.7 eV suggests that the bond with fluoride might be associated with indium instead of phosphorus, because it is much closer to the F 1s peak from InF_3 with In−F at 685.6 eV rather than that from trimethylammonium hexafluorophosphate ($TMAPF_6$) with P−F at 686.8 eV. A blue shift of In 3d XPS peaks toward the same peak from InF_3

DOI: 10.1021/acsnano.8b06692
ACS Nano XXXX, XXX, XXX−XXX

after the HF treatment also supports the reaction of In with HF (Figure 2(b) and Table 1). This is consistent with the blue shift (3 eV) of the In L_3-absorption edge at ~3740 eV and the sharpening of the white line at ~3735 eV in the X-ray absorption near edge structure (XANES)[42] (Figure S5 in the SI). On the other hand, the formation of P−F bonds would be improbable, since the positions of the P 2p peak around 129 eV associated with phosphide are almost constant regardless of the HF treatment and quite different from the P 2p peak from $TMAPF_6$ at 136.5 eV in Figure 2(c). The selective reaction of fluoride with indium is manifested in the time-of-flight secondary ion mass spectrometry (TOF-SIMS) results as well, where signals corresponding only to InF, InF_2, and InF_3 are detected, not those corresponding to PF, PF_2, and PF_3 (Figure S6 in the SI).

Table 1. Binding Energy of XPS Peaks of Pristine and HF-Treated InP QDs, InF_3, and $TMAPF_6$[a]

sample	F 1s	In 3d	P 2p	O 1s
InP		444.6 eV 452.2 eV	128.8 eV	531.8 eV [O1: 531.1 eV, O2: 532.1 eV]
InP−HF	685.0 eV	445.2 eV 452.8 eV	129.2 eV 133.8 eV	532.2 eV [O1: 531.1 eV, O2: 532.2 eV]
InF_3	685.6 eV	446.3 eV 453.9 eV		
$TMAPF_6$	686.8 eV		136.5 eV	

[a]Binding energy of subpeaks of O 1s are written in square brackets.

Formation of In−F bonds can bring about detachment of the organic carboxylate ligands originally bound on the surface In. Sharpening of ^{1}H NMR peaks around 1.6 and 2.3 ppm from the stearate on InP QDs as the HF concentration increases shows that the aliphatic ligands are dropped from the QD surface by the added HF, as shown in Figure 2(e). The XPS O 1s peak at 531.8 eV of pristine InP QD suggests that hydroxides might exist on InP as well as carboxylates, because the O1 subpeak at 531.1 eV with significant intensity is associated with hydroxide-like $In(OH)_3$ or InOOH[6,32] (Figure 2(d)). A blue shift of the O 1s peak to 532.1 eV accompanied by the disappearance of the O1 subpeak after the HF treatment implies that the hydroxide ions are also eliminated. Although O2 represents both $InPO_x$ and carboxylate, the remaining O2 subpeak in InP−HF would mainly originate from $InPO_x$ because carboxylates are effectively removed through the reaction with HF, as shown by ^{1}H NMR (Figure 2(e)), and phosphorus is more oxidized, as checked from the increased XPS P 2p peak at 133.8 eV corresponding to the P−O bond (Figure 2(c) and Table 1). In brief, the HF treatment on InP QDs makes new chemical bonds of the surface indium with fluorine accompanied by the detachment of the organic carboxylate ligands and hydroxides originally bound on the surface indium.

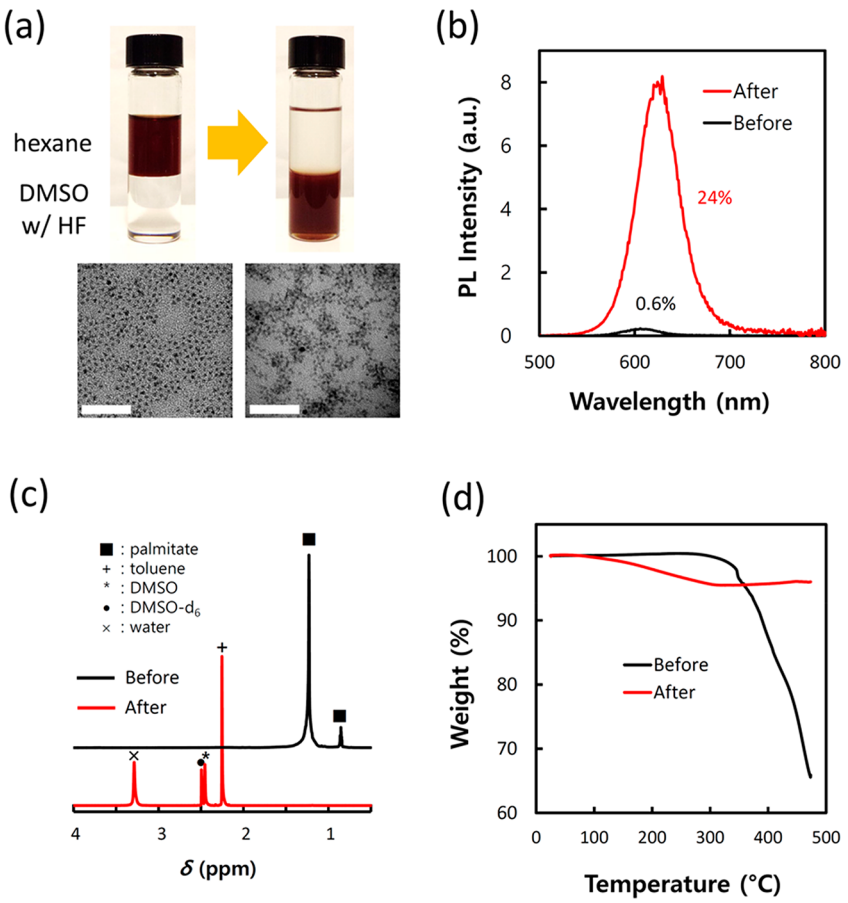

Figure 3. (a) Photographs showing the phase transfer of InP colloidal quantum dots from hexane to 40 mM HF in dimethyl sulfoxide. The corresponding TEM images are shown under the photographs (scale bar: 50 nm). (b) Photoluminescence spectra, (c) ^{1}H NMR spectra, and (d) TGA curves of the QDs before and after the phase transfer.

DOI: 10.1021/acsnano.8b06692
ACS Nano XXXX, XXX, XXX−XXX

To confirm these changes in surface chemistry, phase transfer of InP QDs from a nonpolar to a polar solvent through the photoassisted reaction with HF was performed, because the reaction with highly electronegative fluoride could change the hydrophobic nonpolar surface to a polar one. InP QDs were clearly transferred from hexane to dimethyl sulfoxide (DMSO) with 40 mM HF, as shown in Figure 3(a), and the PLQY increased from 0.7% to 24% (Figure 3(b)). Without HF, InP QDs dispersed in hexane did not transfer to DMSO even with vigorous mixing and photon irradiation for 1 h, which supports that the reaction with HF is the key factor for the phase transfer. ^{1}H NMR peaks coinciding with the palmitate ligand from pristine InP QDs in $CDCl_3$ completely disappeared in the spectrum of the phase-transferred InP QDs in DMSO-d_6, as shown in Figure 3(c). Only traces of the residual toluene, water, and DMSO were detected in the reacted sample. Vibration peaks of the hydrocarbon at ~3000 cm^{-1} and the carboxyl group at ~1500 cm^{-1} in the Fourier transform infrared (FT-IR) spectra had also disappeared (Figure S7 in the SI). In the thermogravimetric analysis (TGA), a much smaller weight loss (about 4%) arising from the evaporation of residual DMSO in the phase-transferred InP QDs than that in the pristine sample (over 35%) agrees well with the elimination of organic ligands (Figure 3(d)). Organic ligands were completely removed by the phase-transfer-based HF treatment, and the resulting surface character was altered to hydrophilic enough to be dispersed in the polar solvent.

Elemental analysis of InP QDs before and after the HF reaction at [HF]/[QD] = 5000 without additional water was quantified by Rutherford backscattering spectroscopy (RBS) with 3.1 MeV acceleration energy in oxygen resonance mode as shown in Figure 2(f) and Table 2. The ratio of In/P is constant regardless of the HF reaction, which also agrees with the value obtained from inductively coupled plasma atomic emission spectroscopy (ICP-AES) (Table 2). The In/P ratio of ~1.4 corresponds to almost 100% In coverage in InP QDs of 3.5 nm diameter, which is based on a spherical quantum dot model consisting of 466 In and 336 P atoms (Figure S8 in the SI). A fully In-covered surface implies that most of the surface traps might originate from In dangling bonds, and the dangling bond related to phosphorus might be insignificant. From the ratio of O/In = 0.81 quantified by RBS, the total amount of the carboxylate and hydroxide groups is estimated to cover roughly 70% of In dangling bonds on the surfaces of pristine InP QDs (SI). The actual coverage of ligands would be smaller because the amount of oxygen might be overly estimated due to the adsorbed oxygen on the carbon substrate. On the other hand, only a ratio of F/In = 0.77 is enough to passivate 92% of total indium dangling bonds as a monovalent X-type atomic ligand (SI). In terms of the ligand density, the fluorides can passivate the surface In dangling bonds more effectively than the aliphatic organic ligands. This might be attributed to the reduced steric hindrance of the single ions similar to other halide ligands such as Cl, Br, and I ions on PbS and PbSe QDs.[4,5,7,8] Please note that PL of InP QDs is improved and the absorption and PL peaks are red-shifted by the reaction with InF_3 dissolved in trioctylphosphine (TOP) as shown in Figure S9 (SI); that is, InF_3 can also work for the surface fluorination on InP QDs. This is like the surface chlorination on PbS QDs using $PbCl_2$ or $CdCl_2$ as Z-type ligands.[1,43] Conclusively, the HF treatment serves as an organic−inorganic ligand exchange process in which the hydrophobic organic ligands are replaced by the fluoride atomic ligands with a higher surface passivation density.

Table 2. Chemical Compositions Extracted from RBS Measurements[a]

sample	In/P	F/In	O/In
InP	1.44 (1.34)		0.81
InP−HF	1.41 (1.37)	0.77	0.42

[a]The In/P values in parentheses were obtained from ICP-AES measurements.

Theoretical Consideration on Fluorinated InP QDs. To verify the thermodynamic preference and the consistency of the photophysical changes such as the red-shifted absorption/PL peaks and the increased quantum yield for PL, and to see if there are any predicted changes in radiative decay rate (oscillator strength) with the surface fluorination, atomistic simulations at the density functional theory (DFT) level were carried out. We applied acetate molecules (Ac) as simplified alternatives of the palmitate ligands used in the experiment. Since hydroxide ions exist on pristine InP QDs as checked by XPS (Figure 2(d)), hydroxide ions are also adopted as one of the ligands to satisfy the electron-counting rule.[6] Figure 4 shows the optimized 2 nm QD structures of $In_{92}P_{68}Ac_{36}OH_{36}$ (InP-Ac/OH) and $In_{92}P_{68}F_{72}$ (InP-F).

From the total energy calculation, we found that the substitution of acetates and hydroxides by fluoride ions is a favorable reaction. The calculated exchange energy is −3.7 eV per fluoride according to the equation

$$E_{exc} = \{E(In_{92}P_{68}F_{72}) + 18E(AcH_2) + 36E(H_2O)\} - \{E(In_{92}P_{68}Ac_{36}OH_{36}) + 72E(HF)\}$$

The sign and magnitude of the energy value implies that the surface fluorination is an exothermic reaction. Accordingly, weak thermal energy might be enough to activate the spontaneous reaction. This is consistent with our finding that the PLQY can be sufficiently increased only by mild heating of less than 100 °C even under dark conditions with no light exposure (Figure S10 in the SI). Differently from the conventional understanding,[35−41] the photoassisted treatment is not a single pathway for the reaction of InP QDs with HF.

As shown in the element-decomposed density of states (DOS) displayed in Figure 4(c,d), both indium and phosphorus contribute similarly to both the valence and conduction bands, indicating the strong covalent bonding character in the InP QDs. F passivation of QD satisfying the electron-counting rules completely eliminates levels in the gap that could act as traps. However, in the case of Ac/OH passivation, some unoccupied intrinsic intragap states remain near the valence band even though the local electron-counting rule is satisfied. This means that pristine InP QDs might have intrinsic nonradiative paths originating due to traps at the surface. The inability of the oxygen-containing ligands to electronically passivate indium is consistent with the general finding on IGS in covalent metal oxides, where dangling bonds of oxygen atoms cannot electronically compensate dangling bonds of the metal cations even when the electron-counting rule is satisfied, resulting in the appearance of IGS.[2,44,45]

In Ac/OH-passivated InP QDs, the conduction band minimum (CBM) and valence band maximum (VBM) are distributed on the surface of the QD with a very minor contribution from the QD interior, as shown in Figure 4(e,g),

DOI: 10.1021/acsnano.8b06692
ACS Nano XXXX, XXX, XXX−XXX

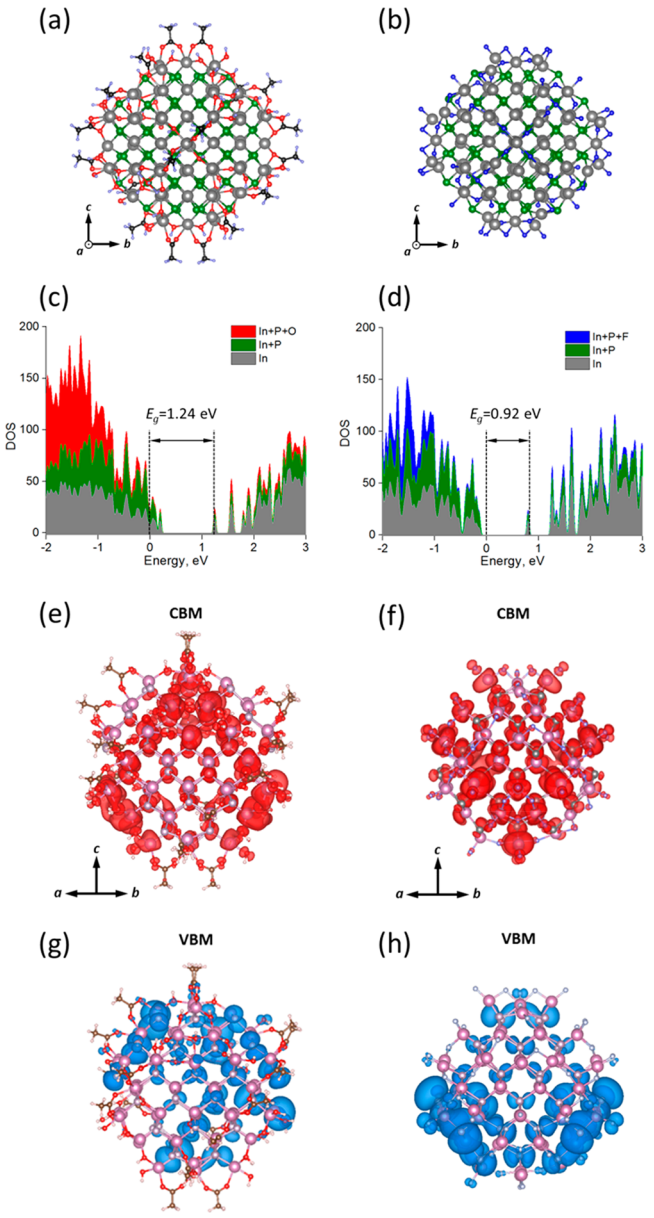

Figure 4. Calculated atomic structures of (a) $In_{92}P_{68}Ac_{36}OH_{36}$ (InP-Ac/OH) and (b) $In_{92}P_{68}F_{72}$ (InP-F) representing the pristine and fluorinated InP QDs. Electron density of states around the band gaps of (c) InP-Ac/OH and (d) InP-F. Electron distributions of the conduction band minimum (CBM) and valence band maximum (VBM) of (e, g) InP-Ac/OH and (f, h) InP-F.

respectively. This is because the band-edge states are located on the surface unpassivated bonds. Upon F passivation, the CBM becomes completely delocalized over the whole QD, while the VBM remains on the QD surface (Figure 4(f,h)). In general, the more delocalized an unoccupied eigenstate, the lower its eigenenergy. Because of the CBM delocalization, the CBM eigenenergy decreases relative to the VBM, causing a significant reduction in the band gap. The band gaps of InP QD with the same inorganic core but different passivating ligands are 1.236 eV for Ac/OH passivation and 0.921 eV for F passivation. Although these band gaps are smaller than the experimentally observed band gaps due to the well-known band gap underestimation in the DFT with the generalized gradient approximation (GGA),[46] the relative change in the band gaps is a reliable quantity. These calculations show that the significant red shifts of the absorption and PL peaks might originate purely from the ligand exchange from the carboxylate/hydroxide to fluorine. We also found that the oscillator strengths of the pairwise electron transitions are changed by the types of ligands determining the shape and symmetry of the QD wave functions. The calculated oscillator strength of the VBM−CBM transition with respect to an average baseline decreases from 0.065 for Ac/OH passivation to 0.042 for F passivation.

The reduction of the oscillator strength by the fluorination could be experimentally validated by comparing the time-resolved photoluminescence (TRPL) properties of pristine InP, HF-treated InP, and InP/ZnS QDs as shown in Figure 5.

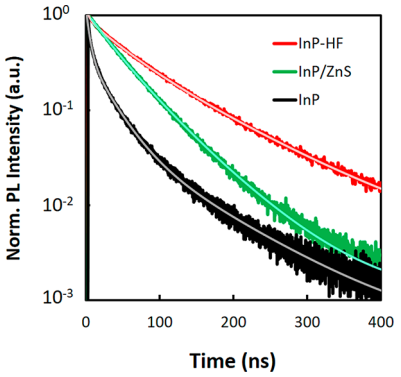

Figure 5. Time-resolved PL curves of pristine InP QDs (black), HF-treated InP QDs (red), and InP/ZnS QDs (green) under 405 nm excitation. Fitted curves (white solid lines) are plotted over the measured.

InP/ZnS QDs were included as a reference with minimal surface traps. The decay curves were fitted with triexponential functions as summarized in Table 3. (Results fitted with stretched exponential function are also included in Figure S11 and Table S1.) Decay behaviors of the three types of QDs based on the same starting InP QDs are quite different. InP QDs with 3.1% PLQY show a fast decay (τ_1) of ~5 ns with 0.41 contribution to the total lifetime, which is known to mainly result from the unpassivated surface traps causing PL quenching.[47,48] Reduced contribution of the fast decay paths and the increased PLQY to 48% in InP-HF QDs ([HF]/[QD] = 5000:1) and to 75% in InP/ZnS implies that the HF treatment as well as the ZnS shell coating can be effective ways to remove the quenching-related traps. It is noteworthy that the average decay time of the HF-treated InP QDs ($\langle\tau\rangle \approx 69$ ns) is longer than that of the InP/ZnS QDs ($\langle\tau\rangle \approx 47$ ns), which results from the significant contribution (0.45) of the slow decay channel ($\tau_3 \approx 108$ ns) despite the faster and larger nonradiative decay term. The longer decay time and the smaller PLQY of InP-HF than those of InP/ZnS lead to its lower radiative transition rate (k_{rad}) as written in Table 3. This means the HF-treated InP QDs might have a weaker luminescence oscillator strength than InP/ZnS QDs, since the oscillator strength is proportional to the radiative transition rate.[49−53]

Fluorination of InAs QDs and Electrical Properties of Solid Films Based on them. From the finding that fluoride effectively passivates In dangling bonds on InP QDs, we expected that fluorination can also work on other In-based QDs such as InAs. To verify the feasibility, InAs QDs were

DOI: 10.1021/acsnano.8b06692
ACS Nano XXXX, XXX, XXX−XXX

Table 3. Values Extracted from Time-Resolved PL Curves in Figure 5 by Fitting with Triexponential Function $I/I_0 = \sum_{i=1}^{3} A_i \exp(-t/\tau_i)$[a]

	τ_1 [ns] (A_1)	τ_2 [ns] (A_2)	τ_3 [ns] (A_3)	τ [ns]	χ^2	QY [%]	k_{tot} [μs^{-1}]	k_{rad} [μs^{-1}]	k_{nrad} [μs^{-1}]
InP	4.8 (0.41)	27.3 (0.52)	93.8 (0.07)	20.7	1.09	3.1	48.3	1.5	46.8
InP/ZnS	15.4 (0.07)	45.5 (0.87)	110.0 (0.06)	46.9	0.98	75	21.3	16.0	5.3
InP−HF	4.8 (0.12)	45.4 (0.43)	108.0 (0.45)	68.8	0.98	48	14.5	7.0	7.5

[a] I and I_0 are PL intensities at time t and 0 ns, respectively; A_i and τ_i are amplitudes and decay times of components, respectively. τ is average decay time, χ^2 is reduced chi square, QY is PL quantum yield, and total decay rates (k_{tot}) are obtained as the inverse of the average decay times. Radiative (k_{rad}) and nonradiative decay rates (k_{nrad}) are estimated from the relationship QY = k_{rad}/k_{tot} where $k_{tot} = k_{rad} + k_{nrad}$.

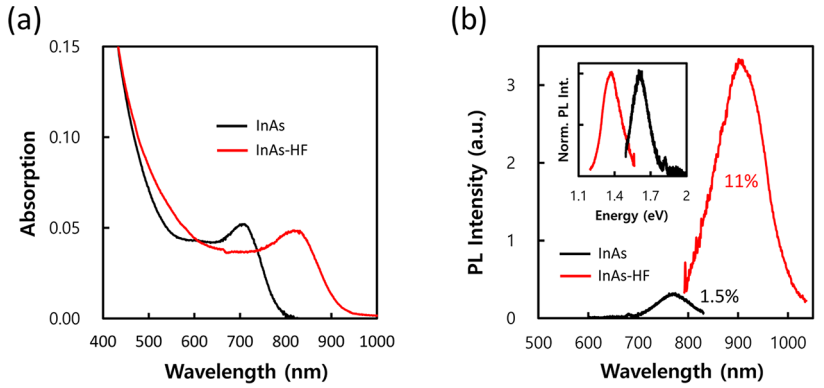

Figure 6. (a) Optical absorption and (d) PL spectra of pristine (black) and HF-treated InAs QDs (red). Inset in (b) shows the normalized PL spectra *versus* energy.

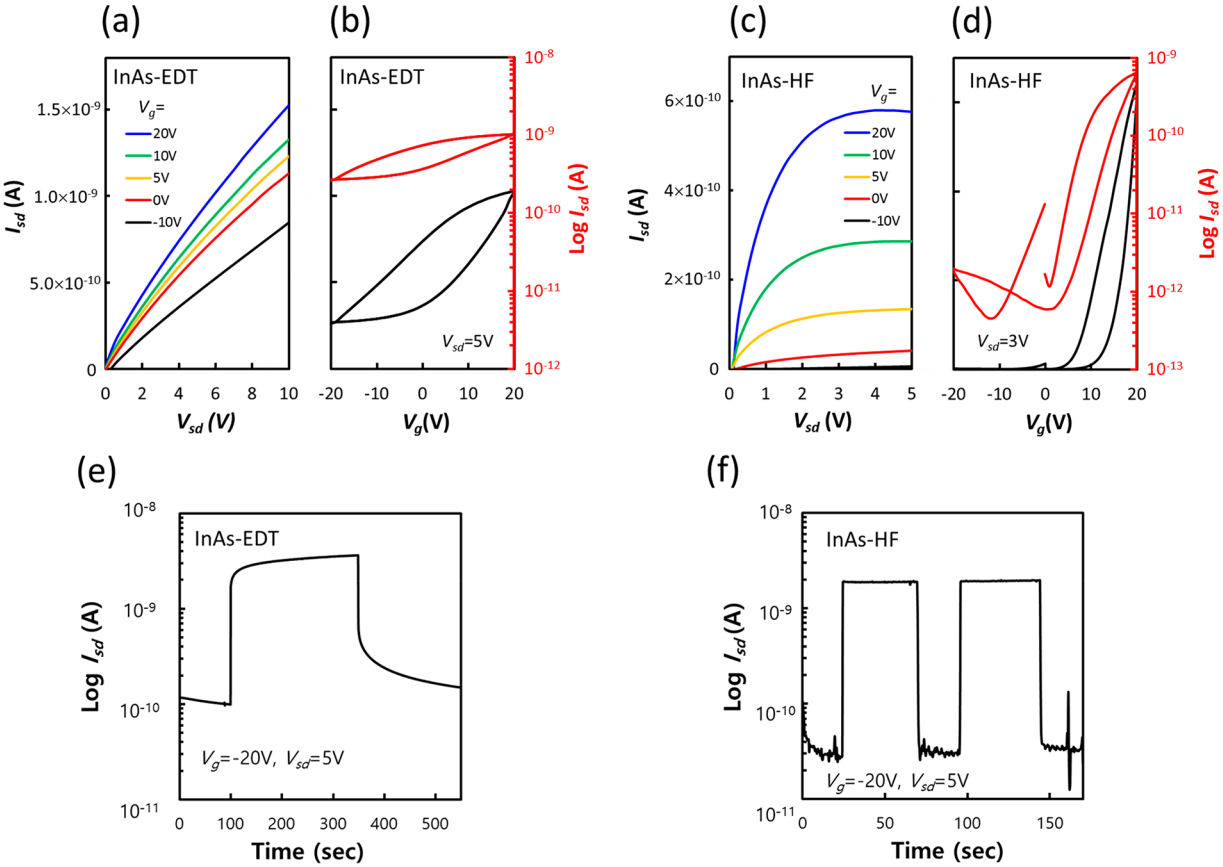

Figure 7. Output and transfer characteristics of (a, b) EDT-treated and (c, d) fluorinated InAs QD (5.1 nm) solid films. Photoresponses of (e) EDT-treated and (f) fluorinated InAs QD (5.1 nm) thin films under the illumination of a white Xe lamp (30 mW/cm^3) at V_{sd} = 5 V and V_g = −20 V.

DOI: 10.1021/acsnano.8b06692
ACS Nano XXXX, XXX, XXX−XXX

synthesized and treated with HF under the same conditions used for InP QDs. As plotted in Figure 6(a,b), both absorption and PL peaks of InAs QDs are red-shifted to lower energies by 0.25 eV, band widths of PL spectra are constant at 0.17 eV, and PLQY increases from 1.5% to 11% after the HF treatment. These results show InAs QDs are also reactive to fluorine and their surface traps associated with PLQY could be reduced by the fluorination. The smaller increase of the PLQY in InAs QDs compared to InP might be attributed to the weaker affinity of the strong hard Lewis base F^- to In^{3+} softened by the bonds with softer As than P, *i.e.*, the chemical symbiotic effect.[1,54] The larger red shift for the InAs QDs (0.25 eV) than that for the InP QDs (about 0.1 eV in Figure 1) is supposed to come from the higher sensitivity of the excitons to the surface state due to the larger exciton Bohr radius of InAs (45 nm) and the smaller particle size (2.8 nm) than those of InP (Bohr radius = 25 nm, particle size = 3.5 nm) or due to the stronger spreading tendency of excitons in the InAs QDs. This result shows PL improvement by HF is not a unique process only for InP QDs and might be extended to other In-based QDs.

Because the fluorination removes the long hydrocarbon chain ligands and efficiently minimizes the surface trap densities on the InAs QD surface, it can be a suitable process for electronic device applications. We examined the charge transport properties of the fluorinated InAs QD-based thin films without any additional molecular linkers and compared them with those of InAs QD thin films treated with 1,2-ethanedithiol (EDT). InAs QDs were fluorinated *via* phase transfer to DMSO as introduced previously. Devices were assembled by a standard spin-casting procedure. The output and transfer characteristics of EDT-treated and fluorinated InAs QD solid films are plotted in Figure 7(a–d). An increase in the source–drain current (I_{sd}) along with the gate voltage (V_g) shown in Figure 7(a) and (c) indicates that both EDT-treated and fluorinated InAs films show unipolar electron transport or n-type behavior. This is because the unpassivated cationic sites provide unbound electrons to the solid films.[3,15,16] In EDT-treated InAs thin films, the current increases quasi-linearly with the source–drain voltage, 0 to 10 V (Figure 7(a)), and is not turned off sufficiently by the gate voltage in the range of −20 to 20 V (Figure 7(b)), which is usually attributed to high carrier concentrations.[15,16] In contrast, the fluorinated InAs QD thin films show clear current saturation (pinch off) in the output curve (Figure 7(c)), and the I_{on}/I_{off} ratio in the same V_g range is ~10^3 with a threshold voltage of 6 V (Figure 7(d)). Electron densities in EDT-treated and fluorinated InAs films derived *via* Ohm's law[16] at V_{th} = 20 V are 7.5 × 10^{17} and 8.7 × 10^{15} cm^{-3}, respectively. The electron doping level of the fluorinated InAs thin film is 2 orders of magnitude smaller than that of the EDT-treated one. The linear mobility is 1 order of magnitude higher in the thin films of fluorinated InAs (2.8 × 10^{-4} $cm^2/V{\cdot}s$) than in the films of EDT-treated InAs (2.3 × 10^{-5} $cm^2/V{\cdot}s$).

Photoresponses of the EDT-treated and fluorinated InAs QD thin films were measured under illumination with a white Xe lamp (30 mW/cm^3) at V_{sd} = 5 V and V_g = −20 V, as shown in Figure 7(e,f). The on/off response time of the photocurrent in EDT-treated thin films is much slower than that in the fluorinated ones. Photocurrent was not saturated even after 250 s illumination, and the dark current also could not be recovered to the level before the illumination even after 200 s in the off state. The slow photoresponse is called persistent photoconductivity, a common problem with InAs QD-based thin films originating from excited carrier trapping and subsequent slow release.[55−57] In contrast, thin films consisting of the fluorinated InAs QDs do not show explicit persistent photoconductivity probably owing to effective passivation of those trapping states. We suggest fluorination of InAs QDs as a way to make a better solid film for visible or infrared photon-sensing devices.[58−60]

CONCLUSIONS

We demonstrated how fluoride ions from hydrofluoric acid can effectively passivate indium dangling bonds on the surface of In-based colloidal QDs in the form of atomic ligands under conditions of lower HF concentration or reduced HF activity, as an alternative mechanism to the accepted surface etching model, which occurs under more vigorous HF treatment. Red-shifted optical absorption and luminescence peaks along with PLQY improvement were observed for the fluorinated InP QDs. Chemical bonding between indium and fluorine was verified using XPS, XANES, and TOF-SIMS analysis, and increased surface coverage by fluoride compared to carboxylate ligands was estimated by Rutherford backscattering spectroscopy. A clear phase transfer of InP QDs from nonpolar hexane to polar DMSO containing HF explicitly confirmed that the aliphatic organic ligands could be entirely exchanged by the fluoride ions through the reaction with HF. Theoretical calculations support the experimental findings: (1) Surface fluorination is an exothermic reaction, which can proceed spontaneously with the assistance of small activation energy. This provided the clue that the fluorination can be successfully achieved by only mild heating, as well as the well-known photochemical treatment. (2) The band gap of InP QDs decreases by the delocalization of the CBM resulting from the surface fluorination, which could explain the observed distinct red shifts of the PL and absorption peaks. (3) The oscillator strength of the VBM−CBM transition decreases through the ligand change from carboxylate/hydroxide to fluoride, which is consistent the longer radiative PL decay times observed for the fluorinated QD compared to the pristine QD. The surface fluorination process could be extended to InAs QDs; that is, the PLQY of InAs QDs increases by an order of magnitude after fluorination as well. Fluorinated InAs QD-based solid films showed better switching properties and an order of magnitude higher electron mobilities than the EDT-treated devices. Moreover, the persistent photoconductivity generally found in InAs QD-based solid films is significantly reduced in the fluorinated devices. The improved properties are directly associated with the effective passivation of surface traps by the fluoride ions as small atomic ligands. These insights are expected to further drive the use of In-based and shell-less QDs in various research and development programs.

METHODS

QD Synthesis and Treatment. *Materials.* All chemicals were used as received without purification: indium acetate ($In(OAc)_3$, 99.99%, Sigma-Aldrich), indium chloride ($InCl_3$, 98%, Sigma-Aldrich), indium fluoride (InF_3, 99.9%, Sigma-Aldrich), palmitic acid (PA, 99%, Sigma-Aldrich), tris(trimethylsilyl)phosphine ($(TMS)_3P$, 95%, Sigma-Aldrich), tris(trimethylsilyl)arsine ($(TMS)_3As$, 99%, Nanomeps), trioctylphosphine (TOP, 90%, Sigma-Aldrich), octadecene (ODE, 90%, Sigma-Aldrich), zinc acetate ($Zn(OAc)_2$, 99.99%, Sigma-Aldrich), hydrofluoric acid (HF, 99.99%, 48 wt % in H_2O, Sigma-Aldrich), oleic acid (OA, 99%, Sigma-Aldrich), trioctylamine (TOA, 98%, Sigma-Aldrich), 1-butanol

DOI: 10.1021/acsnano.8b06692
ACS Nano XXXX, XXX, XXX−XXX

(99.4%, EMD), acetone (99.9%, Sigma-Aldrich), ethanol (99.5%, Sigma-Aldrich), toluene (99.8%, Sigma-Aldrich).

Synthesis of InP QDs. The synthetic method introduced in ref 61 was followed: 0.2 mmol (0.058 g) of $In(OAc)_3$, 0.6 mmol (0.15 g) of PA, and 10 mL of ODE were placed in a flask, subjected to a vacuum state at 120 °C for 1 h, and then heated to 280 °C after the atmosphere in the flask was exchanged with N_2. Then, a mixed solution of 0.1 mmol (29 μL) of $(TMS)_3P$ and 0.5 mL of TOP was quickly injected, and the reaction proceeded for 20 min. The reaction mixture was then rapidly cooled, and acetone was added to produce a precipitate, which was then separated by centrifugation and dispersed in toluene.

Synthesis of InP/ZnS Core/Shell QDs. The synthetic method introduced in ref 62 was followed: 1.2 mmol (0.224 g) of $Zn(OAc)_2$, 2.4 mmol (0.757 g) of OA, and 10 mL of TOA were placed in a flask, subjected to a vacuum state at 120 °C for 10 min, and then heated to 280 °C after the atmosphere in the flask was exchanged with N_2. A toluene dispersion of the InP QDs (optical density of the first excitonic absorption (OD): 0.15, or 1 mL of a 1 wt % toluene solution) was added within 10 s, and then 2.4 mmol of S-TOP was added; the reaction proceeded for 120 min. After that, the reaction mixture was rapidly cooled to room temperature, and acetone was added thereto to produce nanocrystal particles, which were then separated by centrifugation and dispersed again in toluene.

Synthesis of InAs QDs. The synthetic method introduced in refs 63 and 64 was followed: 16 mmol (3.536 g) of $InCl_3$ and 27 mmol (10 g) of TOP were placed in a flask and heated to 120 °C under vacuum for 20 min. Then, the atmosphere in the flask was exchanged with N_2, and the mixture was heated again to a temperature of 260 °C for 10 min to produce an $InCl_3$–TOP mixture. Then, 3 mmol (2.3 mL) of the $InCl_3$–TOP mixture and 2 mmol (0.6 g) of $(TMS)_3As$ were mixed in a glovebox, and the reaction proceeded for 20 min at room temperature to prepare a stock solution. A 5.4 mmol (2 g) amount of TOP was put into a flask and heated to 120 °C for 20 min under vacuum. Then, the atmosphere in the flask was exchanged with N_2. Again, it was heated at a temperature of 300 °C for 10 min, then 1 mL of the stock solution was injected thereto, and the reaction proceeded at 260 °C for 30 min. Finally, the reaction mixture was rapidly cooled to room temperature, and acetone was added to produce a precipitate, which was then separated by centrifugation and dispersed in toluene.

Photochemical Fluorine Treatment. Acetone was added to a toluene dispersion of InP QDs to precipitate the QDs, and the precipitate was centrifuged and then dispersed in toluene at a concentration of 1 μM. A 2.5 mL amount of butanol was added to the vial containing 2.5 mL of the InP QDs dispersed in toluene (2.5×10^{-9} mol). Then 0.5 μL of the HF aqueous solution (1.25×10^{-5} mol, [HF]/[QD] ≅ 5000) was injected into the resulting QD dispersion, and the solution was vigorously mixed and irradiated with white light of 50 mW/cm^2 using a Xe lamp for 30 min. The HF solution was carefully handled in a fume hood with proper protective clothing to avoid exposure to the skin, since it possesses the unique ability to cause deep tissue damage and systemic toxicity. To understand the effect of experimental parameters on the HF treatment, the relative concentrations of HF to QD ([HF]/[QD]) were varied from 0, 10, 100, and 1000 to 10000, and distilled water of the several concentrations (0, 0.4, 1, 2, 4, and 10 vol % of total QD solutions) was intentionally added to the QD solution.

Thermal Fluorine Treatment. The fluorine-passivated InP quantum dots were prepared in the same manner set forth in the photochemical treatment, except that the prepared HF–quantum dot mixture was heated at a temperature of 100 °C for 30 min in the dark with no light, for which the reaction bottle was wrapped with Al foil in a dark room. A HF solution in a syringe was injected through the rubber cap in the dark room.

Fluorine Treatment through Phase Transfer. Acetone was added to a toluene dispersion of the InP QDs to precipitate them, and the aggregated QDs were centrifuged and then dispersed again in 4 mL of hexane to obtain a QD dispersion. Hydrofluoric acid was dissolved in 4 mL of dimethyl sulfoxide (DMSO) to prepare a HF solution (the amount of HF: 4×10^{-4} mol). The first QD dispersion and the HF solution were placed in a Teflon vial together to produce phase-separated bilayers consisting of hexane including InP QDs and DMSO with HF, which were then shaken for 1 min to mix the first QD dispersion and the HF solution thoroughly. The resulting mixture was left alone either under mild heating or under illumination (*e.g.*, white light from a Xe lamp). InP QDs quickly aggregated in the interface between hexane and DMSO right after the shaking and clearly dissolved into the HF–DMSO solution during the irradiation (or the heating).

Fluorine Treatment Using InF_3. A 1 mmol (0.172 g) amount of InF_3 and 22 mmol (10 mL) of TOP were placed in a flask and heated to 100 °C under N_2 for 5 h to produce a 0.1 M InF_3–TOP mixture. A 1 mL amount of the InF_3–TOP mixture was injected to the vial containing 2.5 mL of the InP QDs dispersed in toluene (2.5×10^{-9} mol), and the solution was heated at 100 °C under N_2 for 8 h.

Device Fabrication. *FET Based on InAs QDs Treated with EDT.* A 4 mL amount of a dispersion (QD crude 10 μL + toluene 990 μL) of the InAs QDs with an optical density of 0.15 was washed with acetone and ethanol two times and completely dried for 5 min under vacuum. The dried InAs QDs were moved into a glovebox, and 20 mg of the dried InAs QDs was dispersed in 1 mL of octane and spin-coated onto a SiO_2 (300 nm)/p++-Si substrate having a patterned Au electrode with a channel length of 20 μm to prepare a bottom gate-type field-effect transistor (FET) at 2000 rotations per minute (rpm) for 15 s. The coated QD film was immersed in a 0.03 M EDT acetonitrile solution to repeat a ligand exchange of the oleic acid with the EDT five times to produce a 40 nm thick InAs QD film. After the film fabrication, the FET was heated at 200 °C for 10 min to improve the contact between the QDs and the Au electrode.

FET Based on InAs QDs Treated with Fluorine. F-treated InAs QDs were subjected to a complete phase transfer using a HF solution of DMSO. The F-passivated InAs QDs were spin-coated onto a SiO_2 (300 nm)/p++-Si substrate having a patterned Au electrode with a channel length of 20 μm to prepare a bottom gate-type FET. After the spin-coating, the FET was heated at 200 °C for 10 min to remove the remaining DMSO and improve the contact between the QDs and the Au electrode.

Analysis. Photoluminescence spectra of QDs were obtained using a Horiba Jobin Yvon Triax 320 Fluorolog at an irradiation wavelength of 450 nm. A UV spectroscopy analysis was carried out using a Shimadzu UV-3600 UV spectrometer to obtain a UV–visible absorption spectrum. Quantum yields were determined by measuring the fluorescence intensity of the QDs against rhodamine 6G. Fluorescence lifetime was collected on a Picoquant Fluotime 300 with a PMA 175 detector and an LDH-P-C-405 diode laser with the excitation wavelength of 407.1 nm.

For the ligand analysis, infrared spectroscopy analysis was conducted using a PerkinElmer FT-IR spectrometer, and an NMR spectroscopy analysis was conducted using a Bruker 400 megahertz (MHz) NMR spectrometer.

An inductively coupled plasma-atomic emission spectrometer (manufactured by PerkinElmer Co., Ltd., model name: 5300 PV) and Rutherford backscattering spectroscopy were used to quantify the elements in the QD systems. For RBS analysis pristine and fluorine-treated InP QDs were coated on polished amorphous carbon, and a 3.1 MeV He^{2+} ion beam was irradiated on them at an angle of 22.5° relative to the sample normal in an oxygen resonance mode. The SIMNRA software package was used to simulate the RBS spectra and obtain the composition of the film.

A TOF-SIMS analysis was conducted using a TOF-SIMS V (ION-TOF GmbH, Germany) equipped with a 25 keV Bi^+ ion gun. XPS was conducted using a PHI 5000 Versaprobe spectrometer (ULVAC-Physical Electronics, USA) with a dual-channel neutralizer to compensate the charging of the sample. The binding energy was calibrated from the C 1s peak at 285.0 eV.

Computational Details. The atomic structures were geometrically relaxed using the GGA with the Perdew–Burke–Ernzerhof (PBE)[65] functional as implemented in VASP[66−70] until all forces were less than 0.03 eV/Å. A cutoff energy of 400 eV and vacuum regions of at least 13 Å were used. Since the quantum dots and the molecules are

DOI: 10.1021/acsnano.8b06692
ACS Nano XXXX, XXX, XXX−XXX

0D systems, a single gamma-point was used to sample the Brillouin zone for all calculations.

As we showed in our recent works,[2,6,71] we constructed realistic InP-QD models that correspond to experimental data with $In_{92}P_{68}L^{1-}{}_{72}$ compositions that have a size of 2 nm, the element ratios In/P = 1.35, and In/L^{1-} = 0.78, where L^{1-} refers to the number of charged ligands. This element ratio implies that InP-QDs have a lot of singly bonded In cations on {11−1} facets. Such atoms are usually eliminated during the model construction,[71] but it is necessary to include them for correspondence with experimental data.[73]

Initial configurations of the ligands on the QD surface have been constructed using surface slab models.[6] In ref 6, we also showed that (1) solely oleates and oleic acids cannot pack on the QD surface densely enough for complete QD passivation due to steric hindrance, (2) small ligands are required for complete QD passivation, and (3) during typical acid-precursor synthesis, water molecules provide hydroxyl groups, that serve as small ligands between steric organic ligands. Therefore, we passivate our QDs using both small hydroxyl groups and acetates, represent simplified truncated oleates for computationally efficiency, and denote this passivation as Ac/OH. Structures of $In_{92}P_{68}Ac_{36}OH_{36}$ (InP-Ac/OH) and $In_{92}P_{68}F_{72}$ (InP-F) with about 2 nm sizes are optimized as shown in Figure 4. All ligands are bound to In on the surface, and the electron-counting rule is satisfied.

ASSOCIATED CONTENT

Supporting Information

The Supporting Information is available free of charge on the ACS Publications website at DOI: 10.1021/acsnano.8b06692.

Second derivatives of absorption spectra of pristine and HF-treated InP QDs; TEM images and size distribution of pristine and HF-treated InP QDs; optical absorption and PL spectra of HF-treated InP QDs; In L_3-absorption edge XANES of InP QDs; ToF-SIMS spectra; FT-IR spectra of InP QDs; QD model and surface coverage estimation; absorption and PL spectra of pristine and InF_3-treated InP QDs; PL spectra of thermally HF-treated QDs; time-resolved PL curves fitted with stretched exponential functions (PDF)

AUTHOR INFORMATION

Corresponding Authors

*E-mail: ejjang12@samsung.com.

*E-mail: paul.alivisatos@berkeley.edu.

ORCID

Yehonadav Bekenstein: 0000-0001-6230-5182

A. Paul Alivisatos: 0000-0001-6895-9048

Present Address

[⊥]Department of Materials Science and Solid State Institute, Technion−Israel Institute of Technology, 32000 Haifa, Israel.

Notes

The authors declare no competing financial interest.

ACKNOWLEDGMENTS

The authors acknowledge Prof. Jianbo Gao, Dr. Noah Bronstein, Prof. Son Nguyen, Prof. Changhyun Ko, Dr. André Anders, Ms. Insun Jung, and Dr. Jae Gwan Chung for helpful discussions on quantum dot device fabrication and photophysical/chemical analysis.

REFERENCES

(1) Boles, M. A.; Ling, D.; Hyeon, T.; Talapin, D. V. The Surface Science of Nanocrystals. *Nat. Mater.* **2016**, *15*, 141−153.

(2) Zherebetskyy, D.; Zhang, Y.; Salmeron, M.; Wang, L.-W. Tolerance of Intrinsic Defects in PbS Quantum Dots. *J. Phys. Chem. Lett.* **2015**, *6*, 4711−4716.

(3) Talapin, D. V.; Lee, J.-S.; Kovalenko, M. V.; Shevchenko, E. V. Prospects of Colloidal Nanocrystals for Electronic and Optoelectronic Applications. *Chem. Rev.* **2010**, *110*, 389−458.

(4) Ning, Z.; Ren, Y.; Hoogland, S.; Voznyy, O.; Levina, L.; Stadler, P.; Lan, X.; Zhitomirsky, D.; Sargent, E. H. All-Inorganic Colloidal Quantum Dot Photovoltaics Employing Solution-Phase Halide Passivation. *Adv. Mater.* **2012**, *24*, 6295−6299.

(5) Ning, Z.; Voznyy, O.; Pan, J.; Hoogland, S.; Adinolfi, V.; Xu, J.; Li, M.; Kirmani, A. R.; Sun, J.; Minor, J.; Kemp, K. W.; Dong, H.; Rollny, L.; Labelle, A.; Carey, G.; Sutherland, B.; Hill, I.; Amassian, A.; Liu, H.; Tang, J.; Bakr, O. M.; Sargent, E. H. Air-Stable n-Type Colloidal Quantum Dot Solids. *Nat. Mater.* **2014**, *13*, 822−828.

(6) Zherebetskyy, D.; Scheele, M.; Zhang, Y.; Bronstein, N.; Thompson, C.; Britt, D.; Salmeron, M.; Alivisatos, P.; Wang, L.-W. Hydroxylation of the Surface of PbS Nanocrystals Passivated with Oleic Acid. *Science* **2014**, *344*, 1380−1384.

(7) Bae, W. K.; Joo, J.; Padilha, L. A.; Won, J.; Lee, D. C.; Lin, Q.; Koh, W.-K.; Luo, H.; Klimov, V. I.; Pietryga, J. M. Highly Effective Surface Passivation of PbSe Quantum Dots through Reaction with Molecular Chlorine. *J. Am. Chem. Soc.* **2012**, *134*, 20160−20168.

(8) Woo, J. Y.; Ko, J.-H.; Song, J. H.; Kim, K.; Choi, H.; Kim, Y.-H.; Lee, D. C.; Jeong, S. Ultrastable PbSe Nanocrystal Quantum Dots *via in Situ* Formation of Atomically Thin Halide Adlayers on PbSe(100). *J. Am. Chem. Soc.* **2014**, *136*, 8883−8886.

(9) Murray, C. B.; Norris, D. J.; Bawendi, M. G. Synthesis and Characterization of Nearly Monodisperse CdE (E = Sulfur, Selenium, Tellurium) Semiconductor Nanocrystallites. *J. Am. Chem. Soc.* **1993**, *115*, 8706−8715.

(10) Peng, X.; Schlamp, M. C.; Kadavanich, A. V.; Alivisatos, A. P. Epitaxial Growth of Highly Luminescent CdSe/CdS Core/Shell Nanocrystals with Photostability and Electronic Accessibility. *J. Am. Chem. Soc.* **1997**, *119*, 7019−7029.

(11) Bronstein, N. D.; Li, L.; Xu, L.; Yao, Y.; Ferry, V. E.; Alivisatos, A. P.; Nuzzo, R. G. Luminescent Solar Concentration with Semiconductor Nanorods and Transfer-Printed Micro-Silicon Solar Cells. *ACS Nano* **2014**, *8*, 44−53.

(12) Jang, E.; Jun, S.; Jang, H.; Lim, J.; Kim, B.; Kim, Y. White-Light-Emitting Diodes with Quantum Dot Color Converters for Display Backlights. *Adv. Mater.* **2010**, *22*, 3076−3080.

(13) Coe, S.; Woo, W.-K.; Bawendi, M.; Bulović, V. Electroluminescence from Single Monolayers of Nanocrystals in Molecular Organic Devices. *Nature* **2002**, *420*, 800−803.

(14) Bruchez, M., Jr.; Moronne, M.; Gin, P.; Weiss, S.; Alivisatos, A. P. Semiconductor Nanocrystals as Fluorescent Biological Labels. *Science* **1998**, *281*, 2013−2016.

(15) Hetsch, F.; Zhao, N.; Kershaw, S. V.; Rogach, A. L. Quantum dot Field Effect Transistors. *Mater. Today* **2013**, *16*, 312−325.

(16) Scheele, M.; Engel, J. H.; Ferry, V. E.; Hanifi, D.; Liu, Y.; Alivisatos, A. P. Nonmonotonic Size Dependence in the Hole Mobility of Methoxide-Stabilized PbSe Quantum Dot Solids. *ACS Nano* **2013**, *7*, 6774−6781.

(17) Liu, Y.; Tolentino, J.; Gibbs, M.; Ihly, R.; Perkins, C. L.; Liu, Y.; Crawford, N.; Hemminger, J. C.; Law, M. PbSe Quantum Dot Field-Effect Transistors with Air-Stable Electron Mobilities above 7 $cm^2 V^{-1} s^{-1}$. *Nano Lett.* **2013**, *13*, 1578−1587.

(18) Oh, S. J.; Berry, N. E.; Choi, J.-H.; Gaulding, E. A.; Lin, H.; Paik, T.; Diroll, B. T.; Muramoto, S.; Murray, C. B.; Kagan, C. R. Designing High-Performance PbS and PbSe Nanocrystal Electronic Devices through Stepwise, Post-Synthesis, Colloidal Atomic Layer Deposition. *Nano Lett.* **2014**, *14*, 1559−1566.

(19) Choi, J.-H.; Wang, H.; Oh, S. J.; Paik, T.; Jo, P. S.; Sung, J.; Ye, X.; Zhao, T.; Diroll, B. T.; Murray, C. B.; Kagan, C. R. Exploiting the Colloidal Nanocrystal Library to Construct Electronic Devices. *Science* **2016**, *352*, 205−208.

(20) Clifford, J. P.; Konstantatos, G.; Johnston, K. W.; Hoogland, S.; Levina, L.; Sargent, E. H. Fast, Sensitive and Spectrally Tunable

DOI: 10.1021/acsnano.8b06692
ACS Nano XXXX, XXX, XXX−XXX

Colloidal-quantum-Dot Photodetectors. *Nat. Nanotechnol.* **2009**, *4*, 40−44.
(21) Chuang, C.-H. M.; Brown, P. R.; Bulovic, V.; Bawendi, M. G. Improved Performance and Stability in Quantum Dot Solar Cells through Band Alignment Engineering. *Nat. Mater.* **2014**, *13*, 796−801.
(22) Voznyy, O. Mobile Surface Traps in CdSe Nanocrystals with Carboxylic Acid Ligands. *J. Phys. Chem. C* **2011**, *115*, 15927−15932.
(23) Kim, D.; Kim, D.-H.; Lee, J.-H.; Grossman, J. C. Impact of Stoichiometry on the Electronic Structure of PbS Quantum Dots. *Phys. Rev. Lett.* **2013**, *110*, 196802.
(24) *Official Journal of the European Union* **2003**, *L37*, 19.
(25) Gensch, C.-O.; Baron, Y.; Blepp, M. *Report for the European Commission: Assistance to the Commission on Technological Socio-Economic and Cost-Benefit Assessment Related to Exemptions from the Substance Restrictions in Electrical and Electronic Equipment: Pack 10 Final Report*; May 17, 2016.
(26) Reiss, P.; Carrière, M.; Lincheneau, C.; Vaure, L.; Tamang, S. Synthesis of Semiconductor Nanocrystals, Focusing on Nontoxic and Earth-Abundant Materials. *Chem. Rev.* **2016**, *116*, 10731−10819.
(27) Li, L.; Reiss, P. One-pot Synthesis of Highly Luminescent InP/ZnS Nanocrystals without Precursor Injection. *J. Am. Chem. Soc.* **2008**, *130*, 11588−11589.
(28) Lim, J.; Park, M.; Bae, W. K.; Lee, D.; Lee, S.; Lee, C.; Char, K. Highly Efficient Cadmium-Free Quantum Dot Light-Emitting Diodes Enabled by the Direct Formation of Excitons within InP@ZnSeS Quantum Dots. *ACS Nano* **2013**, *7*, 9019−9026.
(29) Soreni-Harari, M.; Mocatta, D.; Zimin, M.; Gannot, Y.; Banin, U.; Tessler, N. Interface Modifications of InAs Quantum-Dots Solids and their Effects on FET Performance. *Adv. Funct. Mater.* **2010**, *20*, 1005−1010.
(30) Geyer, S. M.; Allen, P. M.; Chang, L. Y.; Wong, C. R.; Osedach, T. P.; Zhao, N.; Bulovic, V.; Bawendi, M. G. Control of the Carrier Type in InAs Nanocrystal Films by Predeposition Incorporation of Cd. *ACS Nano* **2010**, *4*, 7373−7378.
(31) Cros-Gagneux, A.; Delpech, F.; Nayral, C.; Cornejo, A.; Coppel, Y.; Chaudret, B. Surface Chemistry of InP Quantum Dots: A Comprehensive Study. *J. Am. Chem. Soc.* **2010**, *132*, 18147−18157.
(32) Virieux, H.; Le Troedec, M.; Cros-Gagneux, A.; Ojo, W.-S.; Delpech, F.; Nayral, C.; Martinez, H.; Chaudret, B. InP/ZnS Nanocrystals: Coupling NMR and XPS for Fine Surface and Interface Description. *J. Am. Chem. Soc.* **2012**, *134*, 19701−19708.
(33) Tamang, S.; Lincheneau, C.; Hermans, Y.; Jeong, S.; Reiss, P. Chemistry of InP Nanocrystal Syntheses. *Chem. Mater.* **2016**, *28*, 2491−2506.
(34) Mićić, O. I.; Sprague, J.; Lu, Z.; Nozik, A. J. Highly Efficient Band-Edge Emission from InP Quantum Dots. *Appl. Phys. Lett.* **1996**, *68*, 3150−3152.
(35) Talapin, D. V.; Gaponik, N.; Borchert, H.; Rogach, A. L.; Haase, M.; Weller, H. Etching of Colloidal InP Nanocrystals with Fluorides: Photochemical Nature of the Process Resulting in High Photoluminescence Efficiency. *J. Phys. Chem. B* **2002**, *106*, 12659−12663.
(36) Adam, S.; McGinley, C.; Möller, T.; Talapin, D. V.; Borchert, H.; Haase, M.; Weller, H. Photoemission Study of Size Selected InP Nanocrystals: The Relationship between Luminescence Yield and Surface Structure. *Eur. Phys. J. D* **2003**, *24*, 373−376.
(37) Adam, S.; Talapin, D. V.; Borchert, H.; Lobo, A.; McGinley, C.; de Castro, A. R. B.; Haase, M.; Weller, H.; Möller, T. The Effect of Nanocrystal Surface Structure on the Luminescence Properties: Photoemission Study of HF-Etched InP Nanocrystals. *J. Chem. Phys.* **2005**, *123*, 084706.
(38) van Vugt, L. K.; Veen, S. J.; Bakkers, E. P. A. M.; Roest, A. L.; Vanmaekelbergh, D. Increase of the Photoluminescence Intensity of InP Nanowires by Photoassisted Surface Passivation. *J. Am. Chem. Soc.* **2005**, *127*, 12357−12362.
(39) Mnoyan, A.; Kirakosyan, A.; Kim, H.; Jang, H. S.; Jeon, D. Y. Electrostatic Stabilized InP Colloidal Quantum Dots with High Photoluminescence Efficiency. *Langmuir* **2015**, *31*, 7117−7121.
(40) Wang, F.; Yu, H.; Li, J.; Hang, Q.; Zemlyanov, D.; Gibbons, P. C.; Wang, L.-W.; Janes, D. B.; Buhro, W. E. Spectroscopic Properties of Colloidal Indium Phosphide Quantum Wires. *J. Am. Chem. Soc.* **2007**, *129*, 14327−14335.
(41) Byun, H.-J.; Lee, J. C.; Yang, H. Solvothermal Synthesis of InP Quantum Dots and Their Enhanced Luminescent Efficiency by Post-Synthetic Treatments. *J. Colloid Interface Sci.* **2011**, *355*, 35−41.
(42) Figueiredo, M. O.; da Silva, T. P.; de Oliveira, D.; Rosa, D. Indium-Carrier Minerals in Polymetallic Sulphide Ore Deposits: A Crystal Chemical Insight into an Indium Binding State Supported by X-ray Absorption Spectroscopy Data. *Minerals* **2012**, *2*, 426−434.
(43) Ip, A. H.; Thon, S. M.; Hoogland, S.; Voznyy, O.; Zhitomirsky, D.; Debnath, R.; Levina, L.; Rollny, L. R.; Carey, G. H.; Fischer, A.; Kemp, K. W.; Kramer, I. J.; Ning, Z.; Labelle, A. J.; Chou, K. W.; Amassian, A.; Sargent, E. H. Hybrid passivated colloidal quantum dot solids. *Nat. Nanotechnol.* **2012**, *7*, 577−582.
(44) Zherebetskyy, D.; Wang, L.-W. In-Gap States in Electronic Structure of Nonpolar Surfaces of Insulating Metal Oxides. *Adv. Mater. Interfaces* **2014**, *1*, 1300131.
(45) Chadi, D. J. Atomic and Electronic Structures of Reconstructed Si(100) Surfaces. *Phys. Rev. Lett.* **1979**, *43*, 43.
(46) Kurth, S.; Perdew, J. P.; Blaha, P. Molecular and Solid-State Tests of Density Functional Approximations: LSD, GGAs, and Meta-GGAs. *Int. J. Quantum Chem.* **1999**, *75*, 889−909.
(47) Mićić, O. I.; Cheong, H. M.; Fu, H.; Zunger, A.; Sprague, J. R.; Mascarenhas, A.; Nozik, A. J. Size-Dependent Spectroscopy of InP Quantum Dots. *J. Phys. Chem. B* **1997**, *101*, 4904−4912.
(48) Reid, K. R.; McBride, J. R.; Freymeyer, N. J.; Thal, L. B.; Rosenthal, S. J. Chemical Structure, Ensemble and Single-Particle Spectroscopy of Thick-Shell InP-ZnSe Quantum Dots. *Nano Lett.* **2018**, *18*, 709−716.
(49) De Geyter, B.; Justo, Y.; Moreels, I.; Lambert, K.; Smet, P. F.; Van Thourhout, D.; Houtepen, A. J.; Grodzinska, D.; de Mello Donega, C.; Meijerink, A.; Vanmaekelbergh, D.; Hens, Z. The Different Nature of Band Edge Absorption and Emission in Colloidal PbSe/CdSe Core/Shell Quantum Dots. *ACS Nano* **2011**, *5*, 58−66.
(50) Smith, A. M.; Lane, L. A.; Nie, S. Mapping the Spatial Distribution of Charge Carriers in Quantum-Confined Heterostructures. *Nat. Commun.* **2014**, *5*, 4506.
(51) Moreels, I.; Lambert, K.; Smeets, D.; Muynck, D. D.; Nollet, D.; Martins, J. C.; Vanhaecke, F.; Vantomme, A.; Delerue, C.; Allan, G.; Hens, Z. Size-Dependent Optical Properties of Colloidal PbS Quantum Dots. *ACS Nano* **2009**, *3*, 3023−3030.
(52) Jung, J.; Lin, C. H.; Yoon, Y. J.; Malak, S. T.; Zhai, Y.; Thomas, E. L.; Vardeny, V.; Tsukruk, V. V.; Lin, Z. Crafting Core/Graded Shell−Shell Quantum Dots with Suppressed Re-absorption and Tunable Stokes Shift as High Optical Gain Materials. *Angew. Chem., Int. Ed.* **2016**, *55*, 5071−5075.
(53) Leistikow, M. D.; Johansen, J.; Kettelarij, A. J.; Lodahl, P.; Vos, W. L. Size-Dependent Oscillator Strength and Quantum Efficiency of CdSe Quantum Dots Controlled *via* the Local Density of States. *Phys. Rev. B: Condens. Matter Mater. Phys.* **2009**, *79*, 045301.
(54) Pearson, R. G. Absolute Electronegativity and Hardness: Application to Inorganic Chemistry. *Inorg. Chem.* **1988**, *27*, 734−740.
(55) Liu, W.; Lee, J. S.; Talapin, D. V. III-V Nanocrystals Capped with Molecular Metal Chalcogenide Ligands: High Electron Mobility and Ambipolar Photoresponse. *J. Am. Chem. Soc.* **2013**, *135*, 1349−1357.
(56) Fan, J. C.; Lin, Y. J.; Chen, Y. F.; Chen, M. C.; Lin, H. H. Photoconductivity in Self-Organized InAs Quantum Dots. *J. Appl. Phys.* **1998**, *84*, 5351−5353.
(57) Kulbachinskii, V. A.; Lunin, R. A.; Kytin, V. G.; Rogozin, V. A.; Gurin, P. V.; Zvonkov, B. N.; Filatov, D. O. Persistent Photoconductivity in Quantum Dot Layers in InAs/GaAs Structures. *Phys. Status Solidi C* **2003**, *0*, 1297−1300.
(58) Konstantatos, G.; Levina, L.; Tang, J.; Sargent, E. H. Sensitive Solution-Processed Bi2S3 Nanocrystalline Photodetectors. *Nano Lett.* **2008**, *8*, 4002−4006.

DOI: 10.1021/acsnano.8b06692
ACS Nano XXXX, XXX, XXX−XXX

(59) Zhang, Y.; Hellebusch, D. J.; Bronstein, N. D.; Ko, C.; Ogletree, D. F.; Salmeron, M.; Alivisatos, A. P. Ultrasensitive Photodetectors Exploiting Electrostatic Trapping and Percolation Transport. *Nat. Commun.* **2016**, *7*, 11924.
(60) Jeon, S.; Ahn, S.-E.; Song, I.; Kim, C. J.; Chung, U.-I.; Lee, E.; Yoo, I.; Nathan, A.; Lee, S.; Ghaffarzadeh, K.; Robertson, J.; Kim, K. Gated Three-Terminal Device Architecture to Eliminate Persistent Photoconductivity in Oxide Semiconductor Photosensor Arrays. *Nat. Mater.* **2012**, *11*, 301−305.
(61) Battaglia, D.; Peng, X. Formation of High Quality InP and InAs Nanocrystals in a Noncoordinating Solvent. *Nano Lett.* **2002**, *2*, 1027−1030.
(62) Xie, R.; Battaglia, D.; Peng, X. Colloidal InP Nanocrystals as Efficient Emitters Covering Blue to Near-Infrared. *J. Am. Chem. Soc.* **2007**, *129*, 15432−15433.
(63) Guzelian, A. A.; Banin, U.; Kadanich, A. V.; Peng, X.; Alivisatos, A. P. Colloidal Chemical Synthesis and Characterization of InAs Nanocrystal Quantum Dots. *Appl. Phys. Lett.* **1996**, *69*, 1432−1434.
(64) Cao, Y. W.; Banin, U. Growth and Properties of Semiconductor Core/Shell Nanocrystals with InAs Cores. *J. Am. Chem. Soc.* **2000**, *122*, 9692−9702.
(65) Perdew, J.; Burke, K.; Ernzerhof, M. Generalized Gradient Approximation Made Simple. *Phys. Rev. Lett.* **1996**, *77*, 3865−3868.
(66) Hedin, L. New Method for Calculating the One-Particle Green's Function with Application to the Electron-Gas Problem. *Phys. Rev.* **1965**, *139*, A796−A823.
(67) Heyd, J.; Scuseria, G. E.; Ernzerhof, M. Hybrid Functionals Based on a Screened Coulomb Potential. *J. Chem. Phys.* **2003**, *118*, 8207−8215.
(68) Kresse, G.; Joubert, D. From Ultrasoft Pseudopotentials to the Projector Augmented-Wave Method. *Phys. Rev. B: Condens. Matter Mater. Phys.* **1999**, *59*, 11−19.
(69) Kresse, G.; Hafner, J. *Ab initio* Molecular Dynamics for Liquid Metals. *Phys. Rev. B: Condens. Matter Mater. Phys.* **1993**, *47*, 558−561.
(70) Shishkin, M.; Kresse, G. Implementation and Performance of the Frequency-Dependent GW Method within the PAW Framework. *Phys. Rev. B: Condens. Matter Mater. Phys.* **2006**, *74*, 035101.
(71) Zhang, Y.; Zherebetskyy, D.; Barja, S.; Lichtenstein, L.; Bronstein, N. D.; Alivisatos, A. P.; Wang, L.-W.; Salmeron, M. Molecular Oxygen Induced in-Gap States in PbS Quantum Dots. *ACS Nano* **2015**, *9*, 10445−10452.
(72) Voznyy, O.; Sargent, E. H. Atomistic Model of Fluorescence Intermittency of Colloidal Quantum Dots. *Phys. Rev. Lett.* **2014**, *112*, 157401.
(73) Gary, D. C.; Flowers, S. E.; Kaminsky, W.; Petrone, A.; Li, X.; Cossairt, B. M. Single-Crystal and Electronic Structure of a 1.3 nm Indium Phosphide Nanocluster. *J. Am. Chem. Soc.* **2016**, *138*, 1510−1513.

DOI: 10.1021/acsnano.8b06692
ACS Nano XXXX, XXX, XXX−XXX